

# The effect of dust on photometric redshift measurement: a self-consistent technique<sup>\*</sup>

B. Mobasher<sup>1\*\*</sup> and P. Mazzei<sup>2</sup>

<sup>1</sup> Space Telescope Science Institute, 3700 San Martin Drive, Baltimore, MD 21218, USA (mobasher@stsci.edu)

<sup>2</sup> Osservatorio Astronomico, Vicolo dell'Osservatorio 5, 35122 Padova, Italy (mazzei@pdmida.pd.astro.it)

Received 27 April 2000 / Accepted 26 July 2000

**Abstract.** A new method is developed for estimating photometric redshifts, using realistic template SEDs, extending over four decades in wavelength (i.e. from  $0.05 \mu\text{m}$  to  $1 \text{ mm}$ ). The template SEDs are constructed for four different spectral types of galaxies (elliptical, spiral, irregular and starburst), satisfying the following characteristics: a) they are normalised to produce the observed colours of galaxies at  $z \sim 0$ ; b) incorporate the chemo-photometric spectral evolution of galaxies of different types, in agreement with the observations; c) allow treatment of dust contribution and its evolution with redshift, consistent with the spectral evolution models; d) include absorption and re-emission of radiation by dust and hence, realistic estimates of the far-infrared radiation; e) include correction for inter-galactic absorption by Lyman continuum and Lyman forest. Using these template SEDs, the photometric redshifts are estimated to an accuracy of  $\Delta z = 0.11$ .

The simultaneous and self-consistent modelling of both the photometric and chemical evolution of galaxies and the effect of dust, makes this technique particularly useful for high redshift galaxies. The effects on the estimated photometric redshifts, due to assumptions in the evolutionary population synthesis models, are investigated and discussed. Also, the degeneracy in the predicted photometric redshifts and spectral types are examined, using a simulated galaxy catalogue.

**Key words:** galaxies: evolution – galaxies: formation – galaxies: photometry – galaxies: starburst – cosmology: observations

## 1. Introduction

Recent multi-waveband galaxy surveys, carried out from UV to radio wavelengths, have identified a population of rapidly star forming galaxies in the range  $0 < z < 3$  (Sullivan et al 1999; Lilly et al. 1996; Cowie et al. 1997, Rowan-Robinson et al. 1997; Hughes et al. 1998; Mobasher et al. 1999). In particular, these studies confirm a relatively higher rate of star formation

in the past, as supported by the discovery of a population of massive, starforming galaxies at  $z \sim 3$  (Madau et al. 1996; Steidel et al. 1996). These objects are likely to be progenitors of the present day galaxies (Giavalisco et al. 1996; Lowenthal et al. 1997) and hence, a statistical study of this population from the epoch of galaxy formation to the present, gives clues towards scenarios of the formation and evolution of galaxies (Fukugita et al. 1996). This can also constrain the star formation history of galaxies out to  $z \sim 3$ . Such studies require redshift information for a population of starforming galaxies at faint levels. Recently, the depth of the available surveys is greatly extended by the Hubble Space Telescope (HST) observations of the Hubble Deep Fields (HDF). The large spectral coverage of the HDFs provide a unique opportunity to study evolutionary properties of faint galaxies.

Ground-based spectroscopic measurements of the brighter ( $I < 25 \text{ mag.}$ ) sub-sample of the HDF have been performed (Cohen et al. 2000; Steidel et al. 1996; Lowenthal et al. 1997; Zepf et al. 1996). However, for the fainter galaxies in the HDF, redshift measurements are more difficult with spectroscopic features almost impossible to identify. For these objects, the photometric redshift technique (Loh & Spillar 1986; Connolly et al. 1995) is faster than its spectroscopic counterpart and applicable to much fainter magnitudes. This is due to a larger bin size in photometry compared to spectroscopy ( $\sim 1000 \text{ \AA}$  vs.  $1 - 2 \text{ \AA}$ ), leading to a shorter exposure time with a trade-off in accuracy of the measured redshifts.

Considering the new generation of 8m class telescopes, the planned instrumentation on the HST and future, high sensitive radio telescopes, a substantial number of deep surveys at different wavelengths will soon become available. Most of these galaxies will be too faint for spectroscopic study and hence, the photometric redshift technique is the only practical way for estimating their redshifts. In a recent assessment of different photometric redshift techniques, using a redshift-limited spectroscopic survey, it was shown that photometric redshifts can be predicted with an accuracy of 0.1 (0.3) for 68% (99%) of the sources examined (Hogg et al. 1998). Therefore, photometric redshifts could provide a powerful tool for *statistical* studies of evolutionary properties of galaxies and in particular of faint galaxies for which spectroscopic data are difficult to obtain.

<sup>\*</sup> Table 1 is only available in electronic form at the CDS via anonymous ftp to cdsarc.u-strasbg.fr (130.79.128.5) or via <http://cdsweb.u-strasbg.fr/Abstract.html>

<sup>\*\*</sup> Affiliated to the Astrophysics Division of the European Space Agency

The most important step in any study concerning photometric redshift measurement, is the choice of the template Spectral Energy Distributions (SEDs) for different populations of galaxies, with which the observed SEDs should be compared. There are two general ways for adopting the template SEDs:

- a) Empirical templates: in this case one uses the mean *observed* SEDs corresponding to different types of galaxies. The problem here is that there are not enough information about the observed SEDs for different classes of objects at different redshifts (particularly at high redshifts). Therefore, incorporating the spectral evolution of galaxies of different types on their template SEDs is difficult and uncertain.
- b) Synthetic templates: uses model SEDs for different spectral types of galaxies, shifted in redshift space, assuming evolutionary population synthesis models. The main problem here is to constrain the evolutionary model parameters to produce realistic model SEDs (for different types) as a function of redshift. In particular, the effect of dust at high redshifts (specially in star forming galaxies) is not known.

To avoid these problems, we introduce a combined approach, producing realistic model SEDs based on chemo-photometric Evolutionary Population Synthesis (EPS) models, extending from UV to 1 mm in wavelength. The template SEDs here, are consistently and simultaneously optimised to; a) produce the observed colours of galaxies at  $z \sim 0$ ; b) incorporate chemo-photometric evolution for galaxies of different types, in agreement with observations; c) allow treatment of dust contribution and its evolution with redshift, consistent with the EPS models; d) include absorption and re-emission of radiation by dust and hence, realistic estimates of the far-infrared radiation; e) include correction for inter-galactic absorption by Lyman continuum and Lyman forest. *The evolutionary models and hence, the template SEDs, are constrained by minimising the scatter between the photometric and spectroscopic redshifts for a calibrating sample of galaxies with known spectroscopic data.*

The main advantage of this technique over the previous works is that it simultaneously and self-consistently allows for the treatment of both the photometric and chemical evolution of individual galaxies with time. Moreover, since the synthetic template SEDs cover the range from UV to sub-mm wavelengths, one could consistently use the optimised SEDs to estimate contributions from individual galaxies to the far-infrared and sub-mm wavelengths. Also, the effect of dust and its evolution with redshift is self-consistently accounted for in the template SEDs and optimised to produce the observations. This is crucial in any photometric redshift technique if it is to be applied on high redshift, star-forming galaxies (Meurer et al. 1997; Cimatti et al. 1998).

The new photometric redshift technique is outlined in the next section. In Sect. 3, the EPS models are briefly discussed. Sect. 4 presents the calibration sample. This is followed by the optimised template SEDs in Sect. 5. The uncertainties in the photometric redshifts and spectral types are explored in Sect. 6. The conclusions are presented in Sect. 7.

## 2. Photometric redshift technique

For a given galaxy, the photometric redshift can be estimated by comparing its observed SED with a set of template SEDs, corresponding to different morphological types and shifted to different redshifts, accounting for galaxy evolution with look-back time. The redshift and spectral type associated with the template SED closest to the observed SED will then be assigned to that galaxy. The comparison is carried out by minimising the  $\chi^2$  function

$$\chi^2 = \sum_{i=1}^n ((F_{obs}^i - \alpha F_{template}^i) / \sigma^i)^2$$

where the summation,  $i$ , is over the passbands with  $F_{obs}^i$  and  $F_{template}^i$  being, respectively, the observed and template fluxes at a given passband,  $n$ ,  $\sigma^i$  the uncertainty in the observed flux and  $\alpha$  the normalisation, estimated in two different ways. First, it is estimated by forcing the template SED to have the same total energy (calculated by integrating the SED over the observed wavelength range) as the observed SED. Second, the normalisation is used as a free parameter in the fit in minimising the  $\chi^2$ . The two methods give very close results. The comparison between the observed and model SEDs, over the entire range of observed SEDs, will constrain the three free parameters (i.e. redshift, spectral type and normalisation). However, due to changes with redshift in the properties of galaxies, we also need to allow for evolutionary effects on the model SEDs. This introduces more free parameters which will be constrained using observed data, as discussed in the following sections.

In order to construct the template SEDs needed for photometric redshift measurements, we use EPS models, required to estimate changes in properties of galaxies with redshift. These models allow us to develop the template SEDs as a function of redshift for different types of galaxies. In the next section, the EPS models used to derive the template SEDs for different types of galaxies, and their underlying assumptions are discussed. The models are constrained, using observed *local* SEDs for different types of galaxies and by optimising the estimated photometric redshifts to produce their spectroscopic counterparts for a calibrating sample of HDF galaxies with known spectroscopic redshifts. Details of the procedure adopted in this study are summarised in the flow chart in Fig. 1.

## 3. The evolutionary population synthesis models

Synthetic SEDs are constructed following a self consistent procedure, incorporating stellar emission, internal extinction and re-emission by dust. These chemo-photometric EPS models, providing the SEDs extending over four decades in wavelength (ie. from  $0.05 \mu m$  to 1 mm) (Mazzei et al. 1992, hereafter MXD92), allow us to investigate the local properties and the evolution with galactic age of the SEDs of different galaxy types. In particular, we use realistic EPS models for disc galaxies (MXD92), early-type galaxies (Mazzei et al. 1994, hereafter MDX94; Mazzei & De Zotti 1996) and the far-infrared luminous starburst population (Mazzei et al. 1995).

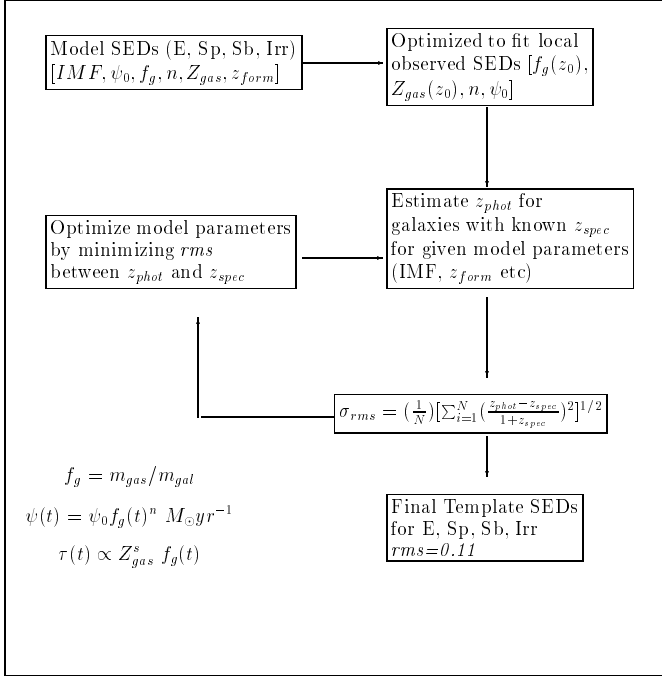


**Fig. 1.** Flow chart summarizing the photometric redshift technique.

In order to match the photometric properties of the galaxy types, expected to dominate deep surveys, we consider 4 different templates, consisting of; elliptical, spiral, irregular and starburst. Details of the SED models for these types and their evolution with cosmic time are given in the above references. In this section, an overview of the main parameters (to be optimized using observed SEDs) will be presented.

The EPS models, used to generate synthetic SEDs for different types of galaxies, have been linked to their chemical evolution so that the increased metallicity of successive stellar generations is taken into account. We adopt a parametrization for the time evolution of the star-formation rate as

$$\psi(t) = \psi_0 f_g^n(t) M_\odot / yr, \quad (1)$$

where  $f_g$  is the fractional mass of gas which takes part in the star formation ( $f_g = m_{gas}/m_{gal}$ ) and  $\psi_0$  is the initial star-formation rate (i.e. SFR at  $z = z_{form}$ ; where  $z_{form}$  is the formation redshift). We assume that initially  $f_g = 1$  with  $m_{gal} = 10^{11} M_\odot$ .

The synthetic spectra for the stellar generations with different metallicities which contribute to the galaxy SED are estimated at any given time, using the recent set of isochrones constructed by Bertelli et al. (1994). These incorporate the results of new stellar evolutionary calculations, based on six metallicity values: 0.0004, 0.001, 0.004, 0.008, 0.02 and 0.05. The isochrones have a fine coverage of masses and ages and include almost all the evolutionary phases from the main sequence to the stage of planetary nebulae ejection or carbon ignition, as appropriate for a given initial mass. This allows us to link the photometric and chemical evolution in galaxies. Further, at any given time and wavelength, the models incorporate both the average correction due to internal extinction by the enriched ISM, as-

suming a dust-to-gas ratio proportional to the gas metallicity and the dust re-radiation from  $3 \mu\text{m}$  up to  $1 \text{mm}$ . We assume that gas and stars have the same distribution. In particular, for spiral, starburst and irregular galaxies we follow the same approach as described in MXD92 (i.e. an exponential function of the galacto-centric radius- see their Eq. (11)) whereas for ellipticals we follow MDX94 (i.e. a density profile given by the King (1966) model). Results are not strongly dependent on the adopted geometry. The evolution of the optical depth,  $\tau$ , follows directly from that of the gas metallicity,  $Z_{gas}$  and  $f_g$  since  $\tau(t) \propto Z_{gas}(t)^s f_g$  (as a consequence of the assumption of a gas-to-dust ratio being proportional to the gas metallicity; MXD92, MDX94). This results in very different histories for the effective optical depths (where  $L_{FIR}/L_{bol} = 1 - \exp(-\tau_{eff})$ ) in the early phases of the evolution of ellipticals in the model, which is based on the adopted IMF parameters.

The IMF and the SFR are the main parameters, controlling the  $e$ -folding star formation time scale, the chemical evolution and, as a direct consequence, the optical depth of the system. Thus, the far-infrared data, where available, are expected to constrain the galaxy metallicity. Therefore, by comparing the local observed SEDs of different galaxy types with models, we constrain both  $\psi_0$  and the IMF. The observed SEDs for nearby spiral and elliptical galaxies with known metallicities and far-IR (IRAS) observations are used to constrain the IMF parameters so that these models successfully reproduce the local chemo-photometric properties of both these types over four decades in wavelength. However, the parameter which is most sensitive to the local properties (i.e. the gas content and optical colours) of galaxies along the Hubble sequence, is the initial star formation rate,  $\psi_0$  (Sandage 1986), which will be constrained for different types of galaxies, using the observed SEDs (Sect. 5.1).

#### 4. The calibration sample

To further constrain the evolutionary parameters in these models, in particular  $n$  and  $z_{form}$ , a calibration sample of HDF galaxies with available spectroscopic redshifts is compiled. The calibration sample contains galaxies bright enough to allow spectroscopic redshift measurements, consisting of both objects with UBVI detections and the UV ‘drop outs’ (i.e. high redshift objects). The advantage of using the HDF galaxies as the calibration sample here is two-fold: (a) HDF galaxies cover the spectral range required for photometric redshift measurement, containing galaxies in the range  $0 < z < 3.5$ ; (b) they are selected using a uniform criteria, for both nearby and distant galaxies, making this an unbiased calibration sample.

The calibrating galaxies are individually inspected and for galaxies with close neighbours, a smaller aperture is adopted to avoid contamination of their light by nearby objects. For the objects with no UV detection (i.e. UV ‘drop outs’), a U-band magnitude of 28.01 mag. was assumed for the photometric redshift measurement. Although this is likely to introduce a bias due to a colour-magnitude relation (i.e. fainter galaxies are bluer), we do not expect it to be significant. This is examined by exploring the range  $28.0 < U < 30.0$  for each of the galaxies in

the UV- drop out sample and estimating their respective photometric redshift. Using models with the same parameters, we find, on average, only a small sensitivity of the estimated photometric redshifts ( $< 3\sigma$ ) to changes in the UV magnitudes in the above range.

The calibrating sample, consisting of 73 galaxies, is listed in Table 1 together with their UBVI photometry and spectroscopic redshifts. The reliability of the spectroscopic redshifts and the photometric accuracy of individual galaxies are discussed in the footnote to this table. The calibration sample in Table 1 was selected to be in the HDF area, to allow accurate UBVI photometry and to have unambiguous spectroscopic redshifts. Moreover, objects with non-stellar sources of energy (i.e. gravitationally lensed candidates; Zepf et al. 1996) are not included. The magnitudes are in the AB system and are measured over an aperture of 3 arcsec diameter (unless stated otherwise in the footnotes to Table 1).

The EPS models for different types of galaxies are therefore further constrained by minimizing the *rms* scatter between the photometric redshifts, predicted by our models, and their spectroscopic counterpart, using the calibration sample in Table 1. Thus, the final EPS models for different types of galaxies, which we define as templates (see below), have local ( $z = 0$ ) SEDs which match the local, observed, SEDs of the corresponding galaxy types and evolutionary properties constrained, using the calibration sample here.

## 5. The template SEDs

### 5.1. EPS model parameters

A large number of EPS models with different input parameters (IMF,  $\psi_0$ ,  $n$  and  $z_{form}$ ) are developed, each accounting for both the local properties and evolutionary behaviour of the 4 types of galaxies considered here. For a given spectral type, the model parameters are normalised at  $z = 0$  by fitting them to the local observed SED of their respective type. The evolutionary behaviour of the EPS models is then constrained by estimating the photometric redshifts to our calibrating sample in Table 1, considering template SEDs with different parameters (i.e. IMF and  $z_{form}$ ) and allowing for Lyman continuum and Lyman forest absorption for  $z > 2$  galaxies. The template SEDs corresponding to the evolutionary parameters which give the closest agreement between the photometric and spectroscopic redshifts are then adopted (see below). The sensitivity of the final results (i.e. photometric redshifts) to the input parameters in the EPS models is studied in the next section while, details of the final templates for individual types, which best satisfy the above requirements, are summarised below:

**a) Ellipticals.** The synthetic SEDs, representing elliptical galaxies, are constructed taking  $n = 0.5$  and  $\psi_0 = 100 M_\odot/yr$ . This gives an *e*-folding star formation time scale of 1 Gyr and reproduces the observed local SEDs for the ellipticals (Fig. 2.1a). A formation redshift of 5 is estimated, corresponding to an age of 13 Gyrs. These models predict a noticeable extinction by dust ( $A_B < 4.6$  mag) in the first stages of their evolution which are

characterized by intense star formation activity, making them powerful far-infrared sources (Fig. 2.2a) (see MDX94 for more details).

**b) Spirals.** The models which produce synthetic SEDs for spiral galaxies have  $n = 2$  and  $\psi_0 = 10 M_\odot/yr$ . They are consistent with an *e*-folding star formation time scale of 10 Gyrs, corresponding to a formation redshift of 2 (i.e. an age of 10-11 Gyrs). This gives a local value of  $L_{FIR}/L_{BOL} = 0.3$ , very similar to that of our own Galaxy. This model re-produces the local SED of NGC 3627 out to the far-infrared wavelengths (Fig. 2.1c). Spiral galaxies are slowly evolving with time ( $L_{FIR}/L_{BOL} < 0.1$  beyond  $z = 1$ ), resulting a smooth evolution for their SED (Fig. 2.2c)- (see MXD92 for more details).

**c) Starbursts.** The template SEDs for the starburst population are produced taking  $n = -1$ ,  $\psi_0 = 2 M_\odot/yr$  and a formation redshift of 5. This template does not produce powerful far-infrared emission at any redshift and hence, its local SED (Fig. 2.1b) is different from that of local luminous far-infrared starbursts (ie. M82 and Arp 220). The SFR in this model is a gradual process with a smooth time scale, leading to formation of very blue, metal poor systems at  $z \sim 0$  (Fig. 2.1b) and a blue, dust-free ( $L_{FIR}/L_{BOL} < 0.05$ ) system at  $z > 1$  (Fig. 2.2b). This mimics a scenario involving frequent but short bursts of star formation, which use a small fraction of gas in these systems (strong bursts of star formation rapidly exhaust the gas, leading to elliptical like systems). The starburst templates here represent the average evolutionary behaviour expected for this population of galaxies.

**d) Irregulars.** The Irregular template has been produced with the same recipe as the starburst but with a formation redshift of  $z_{form} = 1$  (ie. an age of 0.8-0.9 Gyr). The local SED of the irregular galaxy NGC 4449 (Kennicutt 1992) is compared in Fig. 2.1d with our local templates for both irregular and starburst galaxies. These templates are also compared at  $z = 0.975$  (Fig. 2.2d), showing a significant difference beyond  $\lambda \sim 1\mu m$ .

The model SEDs at  $z = 0$  for the four galaxy types discussed above, agree well with the local observed SEDs, as shown in Figs. 2.1a-2.1d. The effects of Lyman break and Lyman forest opacities are included to the template SEDs, using the relations  $\Delta(M)$  vs.  $z$  for different wavelengths, given in Madau (1995). These relations were fitted to parametric forms, which were then used to estimate the respective correction (due to absorption by inter galactic medium) to the SEDs at any given redshift. The correction due to Lyman break and Lyman forest absorption ranges from  $\Delta(M_{UV}) = 0.25$  mag. at  $z = 2$  to  $\Delta(M_{UV}) \sim 1$  mag. at  $z = 2.5$ .

### 5.2. Sensitivity of the template SEDs on the model parameters

In this section we study the dependence of the results (i.e. the photometric redshifts) to the model parameters which most strongly affect the final template SEDs and hence, the predicted photometric redshifts. These parameters consist of the shape of the IMF and its lower mass limit, the total number of tem-

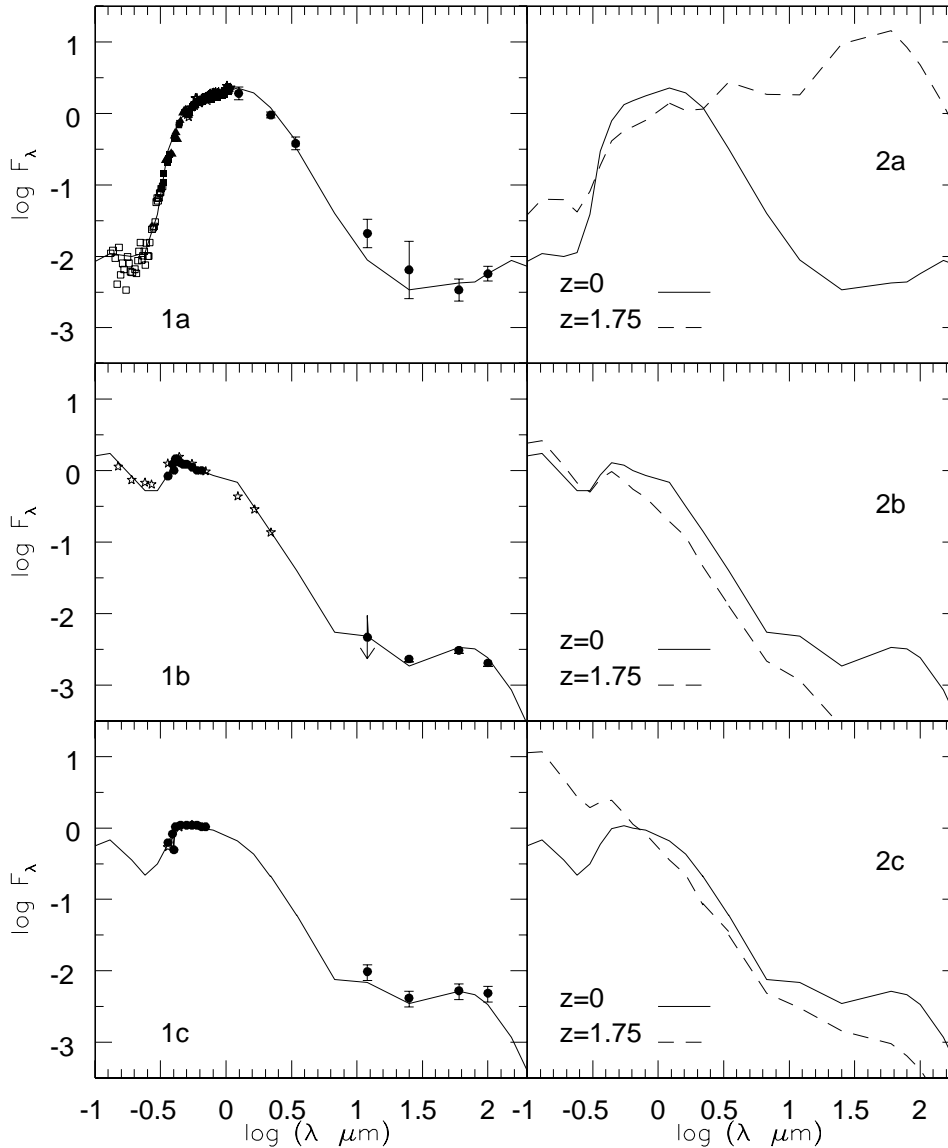


**Fig. 2.1a–c.** The synthetic Spectral Energy Distributions (SEDs) are predicted and constrained to fit the observed data at  $z \sim 0$ , as explained in the text (left panel). Details of each panel and the source of the observational data for each type is given below. **Fig. 2.2a–c.** The local synthetic SEDs for different types of galaxies from Figs. 2.1a–c (solid lines) are compared with their counterparts at  $z \sim 1.75$  (dashed lines).

- a) Elliptical galaxies: open squares (Burstein et al. 1988); filled triangles (Schild & Oke 1971); filled circles (Oke & Sandage 1968); asterisk (Kennicutt 1992); the filled circles at FIR wavelengths correspond to the average local FIR SED for these galaxies (Mazzei & DeZotti 1994b).
- b) Starburst galaxies: this corresponds to the observed SEDs of NGC5996 (MK691). The observed data are taken from: filled circles (Kennicutt 1992); asterisk in the shorter wavelength region (IUE data from Kinney et al. 1993); asterisk in the near-IR region (Balzano 1983); FIR data (IRAS Catalogue Version 2 (Fullmer, L. and Lonsdale, C. 1989)); the IUE data are measured over  $20'' \times 10''$  aperture and are shifted vertically by a factor of 1.6 to normalise to the optical SED; near-IR data, measured over  $10.3''$  aperture has been shifted by a factor of 4.5.
- c) Spiral galaxies: this corresponds to the NGC3627 galaxy. The observed data are from Kennicutt (1992) and Rice et al. (1988).

plates (i.e. spectral types) and the formation redshift for each galaxy type. New template SEDs are generated corresponding to EPS models for elliptical, spiral, starburst and irregular galaxies, using the parameters listed in Table 2, with the rest of the parameters taken to be the same as discussed in Sect. 5.1. For each set of the new templates, the photometric redshifts are estimated for galaxies in the calibrating sample (Table 1) with the *rms* scatter in the quantity  $(z_{phot} - z_{spec})/(1 + z_{spec})$  (i.e. between the photometric and spectroscopic redshifts) calculated and listed in Table 2. The templates corresponding to the model

which gives the smallest *rms* estimate in Table 2 (i.e. model 4) is then adopted. The photometric redshifts estimated for the calibration sample, using the adopted template SEDs (model 4 in Table 2), are listed in Table 1 and compared with their spectroscopic counterparts in Fig. 3. The *rms* scatter of 0.11 here is taken as the uncertainty in the photometric redshift estimates in the range  $0 < z < 3.5$ . The uncertainties in correcting for intergalactic absorption at  $z > 2$  indirectly affect the optimisation of the EPS model parameters in this section. To explore this, we constrained the calibration sample *only* to galaxies with

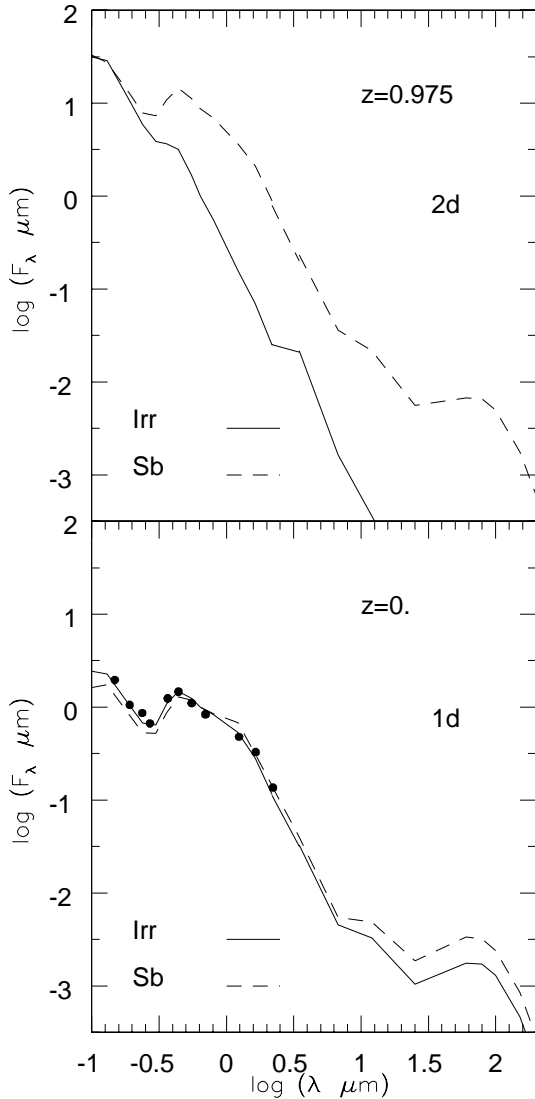


**Fig. 2.1d.** The local observed SED of IRR galaxy NGC 4449 (Kennicutt 1992), filled circles, is compared with the synthetic SED of our Irr template at  $z = 0$  (continuous line) and that for the starburst galaxies (dashed line). **Fig. 2.2d.** The SED for irregulars (solid line) is compared with that for the starbursts (dashed line), both at  $z = 0.975$ .

$z < 2$  (which are much less affected by the IGM absorption) and estimated the EPS model parameters so that to minimise the *rms* scatter in Fig. 3. No change is found in the EPS model parameters. Also, we explored the sensitivity of the *rms* scatter in Fig. 3 to the number of template SEDs used (ie. including templates for different sub-classes of spirals), taking the number of SEDs as a free parameter. This did not reduce the optimum *rms* scatter, derived using the four templates.

Considering the results in Table 2, it seems that one set of models (Salpeter IMF with  $m_l = 0.01M_\odot$ ), give a considerably better fit to observations. This was extensively tested by exploring the parameter space, consisting of the IMF shape and its mass limits, total number of templates and formation redshifts. It was found that this is not due to sampling a particular region of the parameter space or the number of templates, and

**Table 2.** Sensitivity of the *rms* scatter between the photometric and spectroscopic redshifts on the EPS model parameters (i.e. template SEDs)

Model	IMF	$m_l$	Number of Templates	$z_{form}$				<i>rms</i>
				E	Sp	Sb	Irr	
1	Salpeter	0.01	4	5	5	5	1	0.18
2	"	0.01	3	5	5	5	–	0.26
3	"	0.01	3	5	2	5	–	0.24
4	"	0.01	4	5	2	5	1	0.11
5	Salpeter	0.10	4	5	5	5	1	0.27
6	"	0.10	3	5	5	5	–	0.38
7	"	0.10	3	5	2	5	–	0.37
8	"	0.10	4	5	2	5	1	0.22
9	Scalo	0.10	4	5	5	5	1	0.28
10	"	0.10	3	5	5	5	–	0.52
11	"	0.10	3	5	2	5	–	0.45
12	"	0.10	4	5	2	5	1	0.25

is indeed, a real effect. A similar study, using a different set of EPS models and the optimised parameters in Table 2, would be extremely valuable.

The galaxies in the calibration sample in Table 1 also have near-IR data (Fernández-Soto et al. 1999). The above procedure was repeated, using the combined optical and near-IR magnitudes (UBVIJK) for the calibrating sample. This did not change the optimized EPS model parameters in Sect. 5.1 and Table 2. As an independent test of the template SEDs here, we include the near-IR magnitudes to the observed SEDs of the calibrating sample in Table 1 and estimate their photometric redshifts, using the template SEDs predicted in Sect. 5.1 (model 4 in Table 2). Compared to their spectroscopic counterparts, an *rms* scatter of 0.13 is found, in agreement with 0.11 from Fig. 3.

The amount of dust and its evolution with redshift is an important characteristic of the EPS models in this study. This, at any time, is computed self-consistently, accounting for both the SFR and the IMF parameters. By extending the IMF to low  $m_l$  values ( $m_l = 0.01 M_\odot$ ), the gas depletion rate becomes faster, reducing the dust enrichment rate. This leads to higher optical depth in the early evolutionary phase of our elliptical models (templates)-(see also Mazzei & DeZotti 1996 for more details). The UV extinction ( $A_U$ ) corresponding to different IMF and  $m_l$  values is estimated for both elliptical and spiral templates at different redshifts and are listed in Table 3. By changing the shape of the IMF and its lower mass limit, the UV extinction for ellipticals at  $z \sim 2$  changes in the range  $\sim 1 - 4$  mag. Considering the optimised model in Table 2 (model 4), the extinction in spirals is significantly larger than in ellipticals at  $z \sim 0$  while, at higher redshifts ( $z \sim 1.5$ ), ellipticals are obscured more than the spirals. Using our optimised model in Sect. 5.1, the template SEDs at  $z \sim 1.5$  are compared in Fig. 2.2 with their counterparts at  $z \sim 0$ . These show a significant dust contribution to the elliptical SEDs at  $z \sim 1.5$ , as indicated from the peak at the far-IR wavelengths.

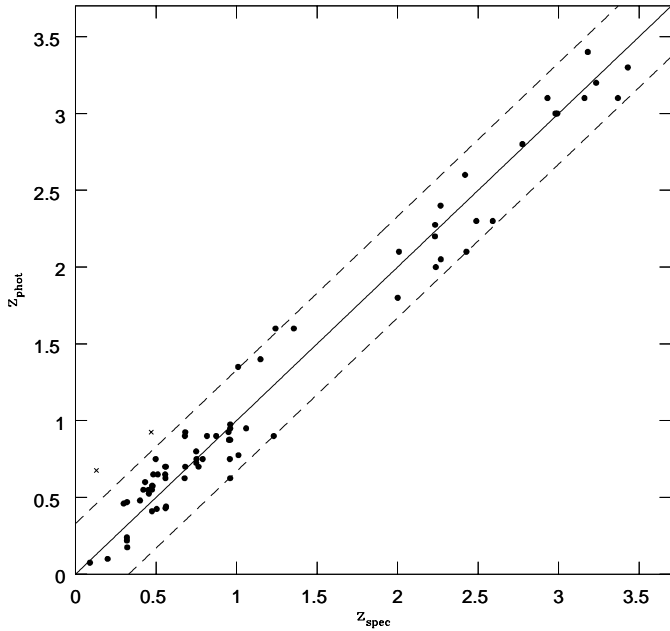


**Fig. 3.** Comparison between the spectroscopic redshifts with the photometric values estimated here for 73 HDF galaxies from Table 1. The spectroscopic redshifts are taken from Cohen et al (1996); Steidel et al (1996); Lowenthal et al (1997); Dickinson (1998). The UV drop-out objects for which a U-band limiting magnitude of 28.01 is used to estimate the photometric redshifts, are also included. The crosses are HDF3646+1408 and HDF3659+1222 galaxies which have uncertain published spectroscopic redshifts of  $z = 0.13$  and  $0.47$  respectively. The lines have a slope of unity. The photometric redshifts are based on model 4 in Table 2. The rms scatter is estimated in  $(z_{phot} - z_{spec})/(1 + z_{spec})$  and corresponds to  $0.11$  with the dashed lines corresponding to  $\pm 3\sigma$  error.

## 6. Uncertainties in the photometric redshifts and spectral types

A potential source of uncertainty in estimating the photometric redshifts and spectral types of galaxies is the possibility that the models might be degenerate (i.e. different synthetic SEDs, corresponding to different redshifts and galaxy types producing the same result). Furthermore, the photometric errors in the observed SEDs are likely to affect the final estimate of both the photometric redshifts and the spectral types of their respective galaxy. Also, due to the relative similarity of the model SEDs for starburst and irregular galaxies (Fig. 2), the accuracy with which the spectral types for these systems are predicted, needs to be established.

To investigate the above problems, a Monte Carlo simulation is performed. A simulated catalogue is generated to resemble the observed HDF survey, with UBVI magnitudes, known redshifts ( $z_{input}$ ) and spectral types. The galaxies are randomly selected to have SEDs similar to the synthetic SEDs for the four types of galaxies (elliptical, spiral, starburst and irregular) considered in Sect. 5.1, shifted in redshift space. Random Gaussian noise, resembling photometric errors, are then added to the simulated SEDs. The simulated catalogue has a magnitude limit of

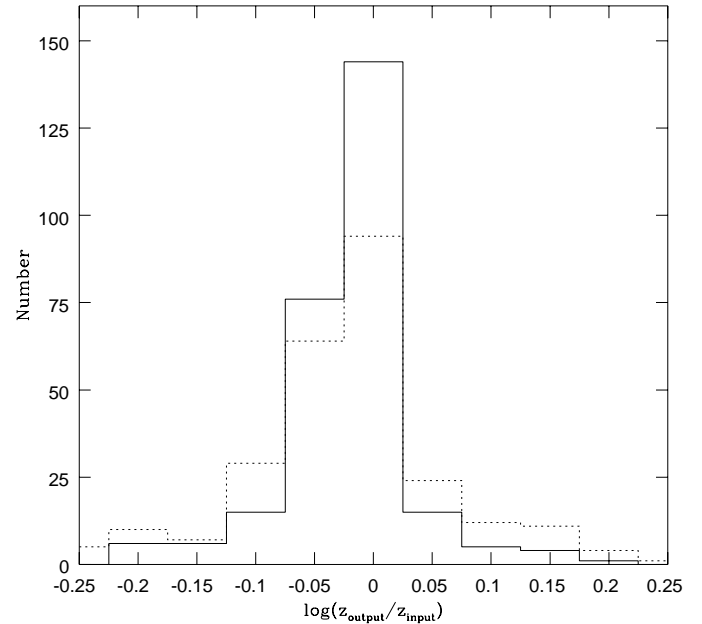


**Fig. 4.** Histogram of  $\log(z_{output}/z_{input})$  for the simulated HDF catalogue. The continuous line is the result for the photometric errors ( $\Delta U$ ,  $\Delta B$ ,  $\Delta V$ ,  $\Delta I$ ) corresponding to  $(0.15, 0.10, 0.05, 0.05)$  and the dotted line corresponds to  $(0.25, 0.15, 0.10, 0.10)$ . Both the histograms peak around zero, implying that the redshifts in the simulated catalogue can be produced to within  $\Delta z = 0.11$ .

**Table 3.** Changes in UV extinction ( $A_U$ ) with redshift, corresponding to EPS models for Elliptical and Spiral galaxies.

redshift	Salpeter IMF $m_l = 0.01 M_\odot$		Salpeter IMF $m_l = 0.1 M_\odot$		Scalo IMF $m_l = 0.1 M_\odot$	
	$A_U(E)$	$A_U(Sp)$	$A_U(E)$	$A_U(Sp)$	$A_U(E)$	$A_U(Sp)$
0	.02	0.78	.02	2.18	.02	2.45
0.5	.44	0.35	.34	1.22	.29	1.44
1	0.67	0.15	.56	0.57	.43	0.70
1.5	2.32	0.04	1.48	0.16	.83	0.20
2.	4.23	–	2.23	–	1.17	–
2.5	4.79	–	2.28	–	1.25	–

$I=28$  mag and an apparent magnitude distribution similar to the observed HDF survey.

The photometric redshift code is used to predict the redshifts ( $z_{output}$ ) and spectral types of individual galaxies in the simulated catalogue and to compare them with their input values. Two set of simulations are carried out, assuming different observational errors (i.e.  $\sigma$  in the Gaussian noise distribution). The difference between the input (simulated) and the output (predicted) redshifts is presented in the histogram in Fig. 4, with the spectral types compared in Table 4.

The  $\log(z_{output}/z_{input})$  distribution (Fig. 4), including *all* the four types of galaxies, shows a distinct peak at zero, indicating that the redshifts for the simulated galaxies are well re-produced within  $\Delta z \sim 0.11$ . The objects, located at the tails

**Table 4.** Results from the simulation of spectral types. Fraction of the galaxies of different types, correctly classified between the input and output simulated catalogues are listed.

	Photometric Errors				E	Percentage <sup>1</sup>		
	$\Delta(U)$	$\Delta(B)$	$\Delta(V)$	$\Delta(I)$		Sp	Sb	Irr
simulation 1	0.15	0.10	0.05	0.05	100%	79%	71%	85%
simulation 2	0.25	0.15	0.10	0.10	100%	66%	49%	62%

<sup>1</sup> Ratio of the number of galaxies of a given spectral type in the output catalogue which are correctly classified, to the total number of galaxies of the same spectral type in the input catalogue.

of the distribution in Fig. 4, are all galaxies classified as spirals, irregulars or starbursts for which, the degeneracy of their SEDs appears to be more serious (see below). When increasing the photometric errors in the simulated SEDs, the agreement between the simulated (input) and predicted (output) redshifts decreases but the distribution still peaks around zero (dotted line in Fig. 4).

The spectral types of the simulated galaxies are compared with the predicted types in Table 4. This gives the ratio of galaxies of a given spectral type, which are correctly classified in the simulation (i.e. galaxies for which their spectral type in the input catalogue were successfully re-produced), to the total number of galaxies of the same type in the input catalogue. In both simulations, we re-produce the spectral types for *all* the ellipticals in the input catalogue with no mis-identifications. However, due to the relative similarity of the UV-to-optical part of the synthetic SEDs for the spirals, irregulars and starburst galaxies (Fig. 2), we can recover respectively 79%, 85% and 71% of the spectral types of galaxies in the input catalogue.

The conclusion from the simulation here is that the photometric redshifts are, on average, well produced (within the expected accuracy) and are not affected by the degeneracy in the template SEDs. Furthermore, the spectroscopic type classification for ellipticals is reliable with 100% re-produced (i.e. no mis-identifications) from the input catalogue while, for the spirals, irregulars and starbursts, there is a slight degeneracy in predicting their spectral types.

## 7. Summary and conclusion

A new technique is developed for estimating the photometric redshifts to galaxies. The advantage of this over the previous methods is that it allows a self-consistent treatment of both photometric and chemical evolution of the template SEDs for different types of galaxies, in agreement with observations. For this reason, the present technique is particularly useful for application to high-redshift galaxies. The template SEDs are constrained to simultaneously satisfy the following criteria: a) produce the observed colours of galaxies at  $z = 0$ ; b) incorporate the spectral evolution for galaxies of different types; c) allow a self-consistent treatment of the dust contribution and its evolution with redshift; d) include correction for inter-galactic absorption by Lyman continuum and Lyman forest. The model parameters are then constrained, using a calibrating sample of HDF galaxies. Using only four optical passbands (UVRI), the photometric

redshifts to galaxies can be estimated with an *rms* accuracy of 0.11. Including near-IR data (UVRIJK), gives a similar *rms* scatter in the photometric redshifts from this method. The sensitivity of the results to different EPS model parameters are explored and the degeneracy of the photometric redshifts and spectral types for galaxies are examined using a simulated catalogue.

## References

- Balzano V.A., 1983, ApJ 268, 602  
 Bertelli G., Bressan A., Chiosi C., Fagotto F., Nasi E., 1994 A&AS 106, 275  
 Burstein D., Bertola F., Buson L.M., Faber S.M., Laurer T.R., 1988, ApJ 328, 440  
 Cohen J.G., Hogg D.W., Blandford R., et al., 2000, ApJ 538, 29  
 Connolly A.J., Csabai I., Szalay A.S., et al., 1995, AJ 110, 2655  
 Cimatti A., Andreani P., Rottgering H., Tilanus R., 1998, Nat 392, 895  
 Cowie L.L., Hu E.M., Songaila A., Egami E., 1997, ApJ 481, L9  
 Dickinson M., 1998, In: Livio M., Fall S.M., Madau P. (eds.) The Hubble Deep Field. Cambridge University Press, Cambridge, p. 219  
 Fernández-Soto A., Lanzetta K.M., Yahil A., 1999, ApJ 513, 34  
 Fukugita M., Hogan C.J., Peebles P.J.E., 1996, Nat 381, 489  
 Giavalisco M., Steidel C.C., Macchetto F.D., 1996, ApJ 470, 189  
 Hogg D., et al., 1998, AJ 115, 1418  
 Hughes D., et al., 1998, Nat 394, 241  
 Kennicutt R.C., 1992, ApJS 79, 255  
 King I., 1966, AJ 71, 64  
 Kinney A.L., Bohlin A.C., Calzetti D., Panagia N., Wyse R., 1993, ApJS 86, 5  
 Lilly S.J., Le Fèvre O., Hammer F., Crampton D., 1996, ApJ 460, L1  
 Loh E.D., Spillar E.J., 1986, ApJ 303, 154  
 Lowenthal J., et al., 1997, ApJ 481, 673  
 Madau P., 1995, ApJ 441, 18  
 Madau P., Ferguson H.C., Dickinson M.E., et al., 1996, MNRAS 283, 1388  
 Mazzei P., De Zotti G., 1994a, MNRAS 266, L5  
 Mazzei P., De Zotti G., 1994b, ApJ 426, 97  
 Mazzei P., De Zotti G., 1996, MNRAS 279, 535  
 Mazzei P., Curir A., Bonoli C., 1995, AJ 110, 559  
 Mazzei P., De Zotti G., Xu C., 1994, ApJ 422, 81 (MDX94)  
 Mazzei P., Xu C., De Zotti G., 1992, A&A 256, 45 (MXD92)  
 Meurer G.R., Heckman T.M., Lehnert M.D., Leitherer C., Lowenthal J., 1997, AJ 114, 54  
 Mobasher B., Cram L., Georgakakis A., Hopkins A., 1999, MNRAS 308, 45  
 Oke J.B., Sandage A., 1968, ApJ 154, 21

Rice W.L., Lonsdale C.J., Soifer B.T., et al., 1988, ApJS 68, 91  
Rowan-Robinson M., et al., 1997, MNRAS 289, 490  
Sandage A., 1986, A&A 89, 101  
Schild R., Oke J.B., 1971, ApJ 169, 209

Steidel C.C., Giavalisco M., Dickinson M.E., Adelberger K., 1996 AJ  
112, 352  
Sullivan M., Treyer M.A., Ellis R.S., et al., 1999, astro-ph/9910104  
Zepf E.S., Moustakas L.A., Davis M., 1996, ApJ 474, L1